Constrained Shrinkage of Highly Oriented Poly(methyl methacrylate) Fibers

Debra D. Wright,[1] Eugene P. Lautenschlager,[2] Jeremy L. Gilbert[3]

[1]*Department of Biomedical Engineering, Michigan Technological University, 1400 Townsend Drive, Houghton, Michigan 49931*
[2]*Division of Biological Materials, Northwestern University, 320 E. Superior Avenue, Chicago, Illinois 60611*
[3]*Department of Bioengineering and Neuroscience, Syracuse University, Link Hall, Syracuse, New York 13244*

Received 27 December 2002; accepted 12 October 2003

ABSTRACT: Constrained shrinkage of fibers is the primary method used to examine orientation in amorphous materials. During the test, fibers are constrained, heated, and the stress that develops is measured as a function of time and temperature. This article describes an apparatus developed to measure that stress and a series of experiments for melt-spun poly(methyl methacrylate) fibers fabricated under three conditions: (1) constant viscosity, (2) increasing temperature, and (3) increasing draw velocity. Results show that both the rates of rise and the decay of the fiber shrinkage stress have an Arrhenius relationship with temperature. Fibers fabricated at a constant viscosity have the same maximum shrinkage stress and rate of stress decay. As the processing temperature decreases or as draw velocity increases, for other parameters held constant, the maximum shrinkage stress increases. The rate of stress rise increases with decreasing processing temperature or increasing draw velocity. Maximum shrinkage stress also increases with increasing molecular orientation when measured by a different test, free heat-induced shrinkage of the fibers. However, it was not possible to correlate both of these results to rubber elasticity theory attributed to the high degree of orientation present in the fibers and high polydispersity in the starting material. © 2004 Wiley Periodicals, Inc. J Appl Polym Sci 91: 4047–4056, 2004

Key words: activation energy; thermal properties; amorphous; fibers; orientation

INTRODUCTION

Melt spinning of poly(methyl methacrylate) (PMMA) has been highly successful at imparting significant molecular orientation and enhancing its mechanical properties. Previous work has characterized the tensile and free shrinkage properties of melt-spun PMMA fibers as a function of processing conditions.[1,2] The work by Wright et al.[2] showed that decreasing the melt temperature, while keeping the other processing variables constant, increased the tensile strength and orientation in the fibers while decreasing the ductility. These fibers have been used to fabricate "self-reinforced composites" (SRC) by a process known as hot compaction.[2–6] This method applies heat and pressure for an appropriate length of time to bond the fibers together. The matrix of the composite is formed directly from the fibers by self-diffusion of polymer chains while under mechanical restraint, hence the term, "self-reinforced." These composites have increased strength, fracture toughness, and fatigue properties compared to those of bulk PMMA and may lead to future improvements in the longevity of total hip replacements.

Although extensive reports have been published on self-reinforced composites,[7–17] optimization of this method depends on empirically selecting the proper time, temperature, and pressure for processing for a particular thermoplastic material. During processing, the fibers are constrained from shrinking along their length. Because the fibers are constrained during hot-compaction processing of composites, characterizing the thermal behavior of fibers while constrained could provide valuable information that would aid in composite processing. In a polymer fiber, the polymer molecules are aligned along the long axis of the fiber. These molecules are in a low entropy state because of their high order. If heat is applied to an unconstrained fiber, the polymer chains will rapidly collapse in a coordinated set of molecular motions and return to a state of high entropy. This results in a change of shapes of the fiber as it shortens in length and increases in diameter. If, however, the fiber is mechanically constrained from shrinking along its length, the polymer relaxation can proceed only by self-diffusion of low-entropy chains back to their random coil configuration. As the entropic force is developed, it can be monitored and measured as a function of time and temperature because of these molecular-relaxation processes.

Correspondence to: D. Wright (wright@mtu.edu).
Contract grant sponsor: American Association for University Women.

Previous work by other investigators[18–27] has examined the shrinkage stress in other oriented materials, but not in highly oriented PMMA fibers. Wide-angle X-ray scattering can be used for oriented amorphous materials, but X-ray crystallography can be used only for crystalline materials; PMMA is totally amorphous. Birefringence can assess the orientation of clear polymers, such as amorphous PMMA, but it is difficult to perform this test for fibrous materials. Mechanical shrinkage stress characterization is an easy and one of the primary methods to examine orientation in amorphous materials.

In an excellent review by Buchanan,[28] free-shrinkage and constrained-shrinkage experiments are summarized. Constrained-shrinkage experiments can be performed at constant or increasing temperature. The fibers characterized in this manner were all semicrystalline materials, and some of the limitations include the analysis of data and the ability to rapidly transfer heat to the sample. Work by others has continued to study semicrystalline materials, in particular poly(ethylene terephthalate),[18–24] poly(ether ether ketone),[25] and other semicrystalline polymers.[26,27] Studies involving oriented PMMA have been limited to films and solid materials with low levels of orientation.[26,29–37,38] Although commercial instruments are available to measure shrinkage stresses, such as the Thermomechanical Analyzer from TA Instruments (New Castle, DE), these devices do not measure the stress as a function of time as the fiber shrinks. These devices also can be cost prohibitive for some labs, and perform multiple analyses that are not necessary for every lab.

Currently, shrinkage in amorphous materials is not well understood,[28] and study of highly oriented PMMA has not been attempted. The goals of this study were twofold:

1. To present an apparatus to measure the shrinkage stresses in constrained fibers.
2. To quantify the shrinkage properties (time constants, maximum shrinkage stresses, and activation energies) of PMMA fibers as a function of time, temperature, and processing conditions.

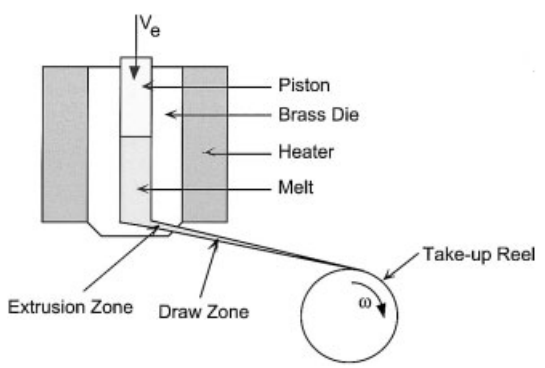

Figure 1 Schematic of melt-spinning apparatus. The extrusion velocity (v_e) is the velocity of the piston.

TABLE I
Processing Conditions for Melt-Spun PMMA Fibers

Processing condition	Processing temperature (°C)	Extrusion velocity, v_e (cm/min)	Draw velocity range, v_d (cm/min)
1	188	0.0127	302–930
2	219	0.0127	302–4081
3	238	0.0127	302–2185
4	213	0.0254	302–4081
5	200	0.0508	302–4081

EXPERIMENTAL

Materials

Extrusion-grade PMMA was obtained from Atohaas (V045, Lot 83,106; Philadelphia, PA) The glass-transition temperature (T_g) was determined to be 107.70 ± 0.56°C (n = 3) using differential scanning calorimetry (DSC; DSC 2920, TA Instruments) at a heating rate of 10°C/min. Previous characterization of V045 by gel permeation chromatography determined a weight-average molecular weight of 212,000 g/mol (polydispersity = 8.3).[39–41]

Fiber spinning

Fibers were processed using a ram-extrusion method illustrated in Figure 1, and described in detail in previous publications.[1,2] A die contains the polymer and piston (1 in. diameter). The polymer was heated and pushed through the die by the piston into a brass spinneret with a 1-mm-diameter hole that was about 3.0 mm in length. The extruded polymer was then pulled onto a take-up wheel to complete the fiber-spinning process. The load on the piston, temperature of the polymer, and speed of the take-up wheel (draw velocity, v_d) were continuously monitored.

Fibers were processed at a constant extrusion rate and constant viscosity. Constant extrusion rate fibers were processed at three temperatures. Viscosity was characterized using simple tube flow equations and was kept constant by varying the extrusion speed and melt temperature. Three constant viscosity conditions were identified. In both cases, fibers were fabricated using the maximum available speeds for the take-up wheel. There were five unique processing conditions for fiber processing, as summarized and numbered in Table I. These five fiber types allowed us to study three independent processing variables: temperature of the polymer (processing conditions 1–3), take-up wheel velocity (processing condition 2), and melt viscosity (processing conditions 2, 4, and 5). Diameter of

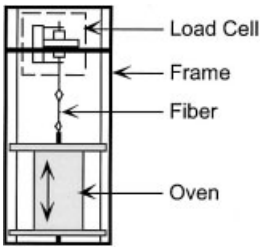

Figure 2 Schematic of fiber-shrinkage device. The main components are a load cell, frame, and oven. The oven was mounted on a movable platform that was counterweighted. The fiber was placed in two grips as shown. The bottom grip passes through the oven and was attached to the frame.

the resultant fibers was measured using an optical microscope.

Constrained fiber shrinkage apparatus

The apparatus used to measure fiber shrinkage is pictured in Figure 2. It is inexpensive to fabricate and measures the force developed in a shrinking fiber as a function of time at a constant temperature. Its main components were a frame, stationary load cell, and cylindrical oven mounted on a movable platform. The movable platform was counterweighted and had bearings to allow for easy and quick movement of the oven. A brass rod was suspended from the load cell and attached to an alligator clip that served as the top grip for the fiber. This brass rod was surrounded by a ceramic tube for insulation, and an aluminum convective heat shield to protect the load cell from excessive heat was attached to the ceramic tube. The bottom grip was also an alligator clip, and was attached to a screw threaded rod that passed through the oven and was attached to the frame of the device. Two J-type wire thermocouples were located inside the oven, at the top and bottom of the sample. The load cell was cooled by a small fan attached to a ring stand separate from the frame of the device. The force and temperature voltage signals were recorded using a computer with an A/D board (Model AT-MIO-16F; National Instruments Corp., Austin, TX) and custom-written programs (LabWindows, version 2.3a, National Instruments).

The load cell is pictured in more detail in Figure 3, along with a representative calibration curve. The measuring device was a linear variable differential transformer (LVDT). Brass cantilevers (53 × 10 × 0.4 mm) were attached to the base of the load cell as well as to the iron core inside the LVDT. The load cell was calibrated by hanging weights of a known mass on the load cell and measuring the change of voltage, as shown in Figure 3. The load cell was calibrated before testing began, and the value used in this set of experiments was 10.95 mg/mV. Altering the stiffness of the

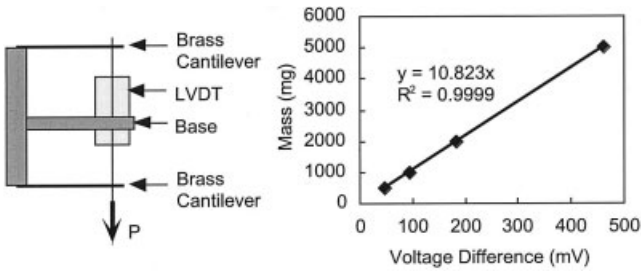

Figure 3 Detail of load cell and representative calibration curve.

brass cantilevers can change the sensitivity and load range of the load cell.

One concern with this apparatus was that the loads measured should be indicative of fiber-shrinkage processes, and not of the expansion or contraction of the device itself. The oven was preheated, and was therefore heating a portion of the metal rod that serves as the stationary grip. Once the oven was raised, this portion of the rod was allowed to cool, and the portion of the grips around the fiber was allowed to heat. To ensure that the loads measured were indicative of fiber-shrinkage events, the grips were attached to one another with no fiber in between them. The oven was set at 125°C, raised, and the force was measured as a function of time. This temperature was chosen because preliminary tests showed that it was at this temperature that the tests began to last longer than just a few minutes. At this temperature, the fiber-shrinkage events last long enough that an equilibrium status was reached with the expansion and contraction of the device itself.

The results of this validation test are shown in Figure 4. It can be seen that the apparatus exerted a compressive stress on the load cell, and that the displacement was approximately 100 μm. It is important to note that in all of the preliminary fiber-shrinkage tests, only tensile forces were measured. Additionally, a displacement of 100 μm resulted in a strain of less than 0.5% in a fiber the length of the test specimen

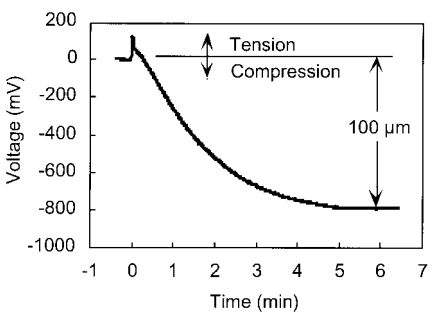

Figure 4 Results of validation test for the fiber shrinkage apparatus at 125°C. The grips were attached to one another, and the resultant voltage was measured.

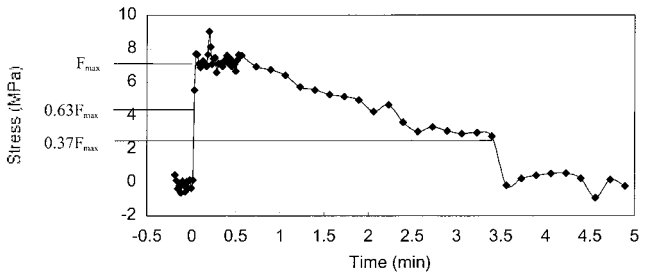

Figure 5 Typical fiber shrinkage result from previously published work.[43] Three fibers are used in this sample, and the temperature of the test is 150°C. The fibers fracture at just under 3.5 min.

(2.54 cm). This strain, especially at an elevated temperature, was expected to exert very little compressive stress on a fiber. The fiber unconstrained shrinkage ratio (heat relaxation ratio, HRR[1]) was on the order of 10 : 1 or higher, indicating shrinkage strains of 1000%. Therefore, for purposes of this analysis, the apparatus was assumed to contribute negligible stress to the fiber, and its contribution was ignored.

Constrained fiber shrinkage testing

To perform a constrained fiber shrinkage test, a length of fiber about 2.75 cm long was cut and heat-resistant tape was placed on each end. The heat-resistant tape provided a surface for the grips to attach to the fiber. The exposed fiber was measured with a digital caliper and was nominally 2.54 cm long. The nominal diameters ranged from 30 to 100 μm. The fiber was placed in the grips so that there was no tension on the fiber before the test was begun. Data acquisition then began, and these points provided the baseline voltage at zero load. After approximately 5 s, the oven was raised in 2–3 s. The time required to raise the oven was recorded for each sample. The gain, or sensitivity, of the A/D board was adjusted for each sample so that the maximum resolution of the signal was attained. One fiber was used in each test.

Fibers were tested at six temperatures in the range from 75 to 185°C. At all temperatures $>$ 75°C, five samples were tested. Two samples were tested at 75°C. Three samples were tested at 75°C if the two samples were not reproducible.

Data analysis

A typical constrained fiber shrinkage graph from preliminary work is shown in Figure 5. The stress in the fiber was calculated by

$$\sigma = \frac{F}{\frac{\pi}{4}D^2} \tag{1}$$

where σ is the stress in the fiber, F is the force developed in the fiber, and D is the diameter of the fiber. The stress begins at zero, rises to the maximum shrinkage stress σ_{max} and then may decay. The stress decays to zero at higher temperatures. For the particular sample depicted in Figure 5, the fiber breaks at about 3.5 min. At lower temperatures, the stress may remain at σ_{max} or may slightly decay, but not back to zero. For the purposes of analysis, it was assumed that during the rise and decay of the stress, there was an exponential relationship between the stress and the time elapsed. For the rise of the stress, this can be written as

$$\sigma = \sigma_{max}(1 - \exp^{-t/\tau_R}) \tag{2}$$

where σ is the stress in the fiber at a specified time t, and τ_R is the time constant of the rise process. It is hypothesized that this time constant is related to the Rouse relaxation time, which is the time required for initial motion of polymer chains.[42] The time constant of the rise process was determined by setting $t = \tau_R$, and solving for σ. Solving for σ yields that when $t = \tau_R$, $\sigma = 0.63\sigma_{max}$. Therefore, by knowing the maximum stress, one can then determine the time at which the stress was 63% of the maximum stress. This time was the time constant for the rise process (τ_R).

A similar analysis explains the decay process of the stress. The decay process can be written as

$$\sigma = \sigma_{max}\exp^{(t_{max} - t)/\tau_D} \tag{3}$$

where t_{max} is the time at the maximum stress and τ_D is the time constant for the decay process. This time constant is hypothesized to be related to the disengagement time for polymer molecules, which is the time necessary for complete reptation of the molecules out of their entanglement network.[42] Equation (3) can also be written as

$$\sigma = \sigma_{max}\exp^{t_{max}/\tau_D}\exp^{-t/\tau_D} \tag{4}$$

It can be seen in eq. (4) that, as long as t_{max} is much less than τ_D, eqs. (3) and (4) can be simplified to

$$\sigma = \sigma_{max}\exp^{-t/\tau_D} \tag{5}$$

The time constant of the decay process can then be determined as for the rise process by setting $t = \tau_D$, and solving for σ. Solving for σ yields that when $t = \tau_D$, $\sigma = 0.37\sigma_{max}$. Therefore, by knowing the maximum stress, one can then determine the time at which the stress was 37% of the maximum stress. This time was the time constant for the decay process (τ_D).

A Visual Basic program was developed (Microsoft Excel, Macintosh Office 98) that would determine the average oven temperature, maximum stress, time at maximum stress, rise time constant, and decay time

TABLE II
Maximum Stresses and Activation Energies for PMMA Fibers in Constrained Fiber Shrinkage

Independent variable (processing condition)	Draw velocity, v_d (cm/min)	Processing temperature (°C)	Extrusion velocity, v_c (cm/min)	Maximum stress (MPa)	E_A (kJ/mol)	
					Rise process	Decay process
Processing temperature						
1	302	188	0.0127	6.99 ± 0.27	103.8 ± 6.8	147.5 ± 16.2
2	302	219	0.0127	1.36 ± 0.07	127.7 ± 8.4	177.2 ± 19.0
3	302	238	0.0127	0.59 ± 0.07	112.5 ± 9.0	179.9 ± 19.0
Draw velocity						
2	302	219	0.0127	1.36 ± 0.07	127.7 ± 8.2	177.2 ± 11.8
2	1401	219	0.0127	5.74 ± 0.33	194.3 ± 13.3	143.6 ± 14.3
2	2594	219	0.0127	11.23 ± 1.96	153.3 ± 12.8	159.9 ± 14.8
Constant viscosity						
2	2594	200	0.0508	13.51 ± 0.76	—[a]	82.4 ± 14.0
4	2594	213	0.0254	11.59 ± 0.30	—[a]	96.4 ± 22.1
5	2594	219	0.0127	11.23 ± 1.96	—[a]	159.9 ± 15.7

[a] Insufficient data were obtained to make an accurate estimate of this parameter.

constant from the raw data. The average temperature in the oven was determined using trapezoidal numerical integration over the time interval $0 \leq t \leq \tau_D$. If the stress in the fiber specimen did not decay during the testing period, the time interval used was $0 \leq t \leq 3\tau_R$. Because the sampling rate was 20 Hz, times that were predicted to be lower than 0.05 s were not considered valid measurements and were discarded. All data were examined for outliers, and in certain cases, times, stress, and/or temperatures were calculated by hand because of data analysis or acquisition complications.

To analyze the rise and decay time constants, an Arrhenius relationship was assumed to exist between the time constant and the oven temperature. The Arrhenius equation relates the rate of the process to the inverse of the temperature and can be written in the form

$$\frac{1}{\tau} = A\exp\left(-\frac{E_A}{RT}\right) \tag{6}$$

where τ is the time constant of interest (min), A is the frequency factor, E_A is the activation energy of the process (J mol^{-1}), R is the universal gas constant (8.314 J mol^{-1} K^{-1}), and T is the absolute temperature (K). By taking the natural log of each side of the equation, it can be written as

$$\ln\frac{1}{\tau} = \ln A - \frac{E_A}{R}\frac{1}{T} \tag{7}$$

where it can be seen that if the data follow an Arrhenius relationship, plotting $\ln(1/\tau)$ versus $1/T$ will yield a straight line. The slope of this line represents the activation energy of the development or decay of the stress.

A one-way analysis of variance (ANOVA) was performed to determine the differences between maximum stresses in each of the three groups listed in Table II. The independent variable was the processing condition that was varied and the dependent variable was the maximum stress developed. For the ANOVA, only maximum stresses > 100°C were considered. A Newman–Keuls *post hoc* test was used to determine differences between the groups. A $p \leq 0.05$ was considered significant.

RESULTS AND DISCUSSION

A fiber-shrinkage test yields three pieces of information about a constrained fiber while it is heated. First, the maximum stress (σ_{max}) obtained during heating as a function of temperature can be determined. Second and third, the time constants associated with the development (rise time constant, τ_R) and decay (decay time constant, τ_D) can also be determined as a function of temperature.

Figures 6 to 8 show the results of the maximum stress versus temperature for the five groups of fibers tested. Generally, the maximum stress is constant versus temperature. In Figure 6, however, it can be seen that the maximum stress first increases and then decreases slightly with temperature for the sample processed at 188°C. For the sample with the highest draw velocity (and therefore smallest diameter), a decrease in the maximum stress is seen at the higher temperatures (e.g., Fig. 6 at 188°C and Fig. 8 at 219°C). This was also seen in previous work with commercially fabricated fibers.[43] At temperatures < 100°C, the temperature was seen to remain constant in most cases, but it also increased in Figure 7 for samples drawn at 1401 cm/min and decreased in Figure 6 for samples

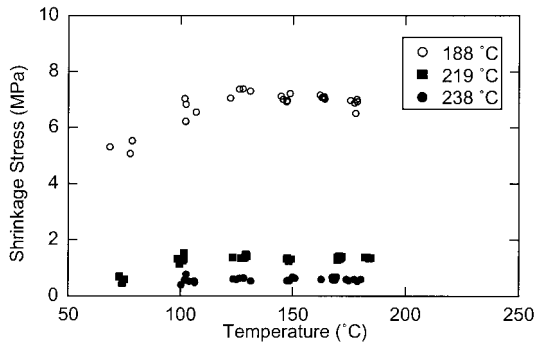

Figure 6 Fiber maximum stress versus temperature with respect to the effect of processing temperature. The fibers were all fabricated at a draw velocity of 301 cm/min and extrusion velocity of 0.0127 cm/min. The processing temperatures are as shown in the legend.

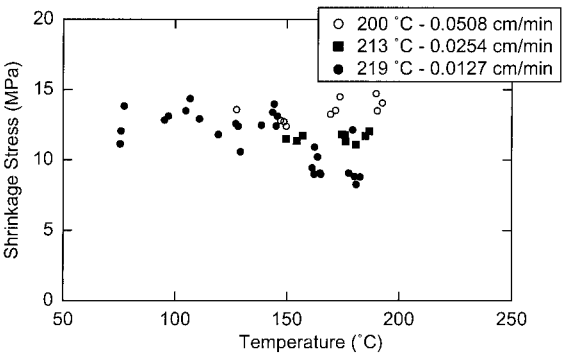

Figure 8 Fiber maximum stress versus temperature with respect to the effect of constant viscosity. The fibers were all fabricated at a constant nominal viscosity of 6.3E6 Pa s. The processing conditions (melt temperature and extrusion velocity) are as listed in the legend.

drawn at 188°C. Table II lists the means and SD values of the maximum stress for each fiber type. Figure 8 shows that maximum stresses were equal at test temperatures < 150°C, but diverged at higher temperatures for fibers made at different temperatures and draw rates but equal viscosities.

The statistical analysis found several significant results when comparing the maximum stress values of the three groups. As the processing temperature decreased, the maximum stress increased when all other variables were held constant. As the draw velocity increased, a statistically significant increase was seen in the maximum stress when all other variables were held constant. Finally, when fibers were fabricated at a constant viscosity, the fibers fabricated at 200°C had a higher maximum stress than that of the other two groups that were fabricated at higher temperatures when tested above 150°C.

Arrhenius plots for the time constants for each of the three groups are shown in Figures 9 to 11. These results are plotted on a common log y-scale because of the ease in interpreting results. The x-axis is in K^{-1}, and the top axis is labeled in degrees Celsius. Note that low temperatures are on the right side of the graph, and short times are at the top of the graph. Regression lines are shown with 95% confidence intervals, and the rise time constants lie above the decay time constants. Regression lines were fit to the natural log value for determination of the activation energies listed in Table II. Activation energies were also determined for the V045 polymer from dynamic rheometry experiments.[44] The values obtained from dynamic rheometry (155.7, 164.6, 156.8 kJ/mol) show good agreement to the values shown in Table II. Values for the activation of the rise process for samples fabricated at a constant viscosity are not available. These fibers were tested only at high temperatures, and not enough low temperature data points were collected to make a good estimate for this activation energy. At high temperatures, the time for the rise process was too short to be measured by the instrument developed for this study.

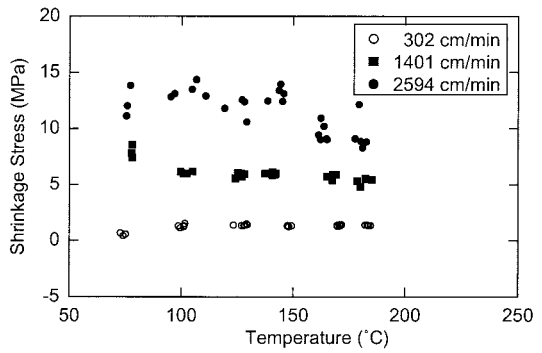

Figure 7 Fiber maximum stress versus temperature with respect to the effect of draw velocity. The fibers were all fabricated at a melt temperature of 219°C and extrusion velocity of 0.0127 cm/min. The draw velocities are as shown in the legend.

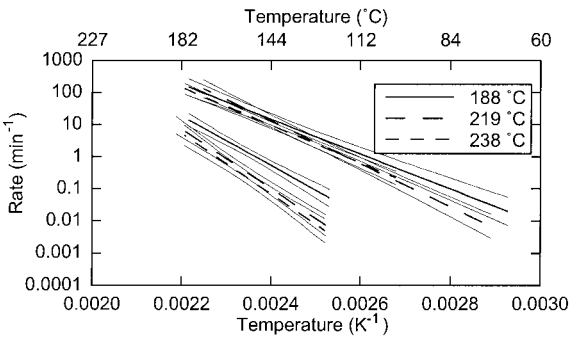

Figure 9 Arrhenius plots depicting the effect of processing temperature. The rise curves lie above the decay curves. The fibers were all fabricated at a draw velocity of 301 cm/min and extrusion velocity of 0.0127 cm/min. The melt temperatures are as shown in the legend. For clarity, only regression lines and 95% confidence intervals are shown.

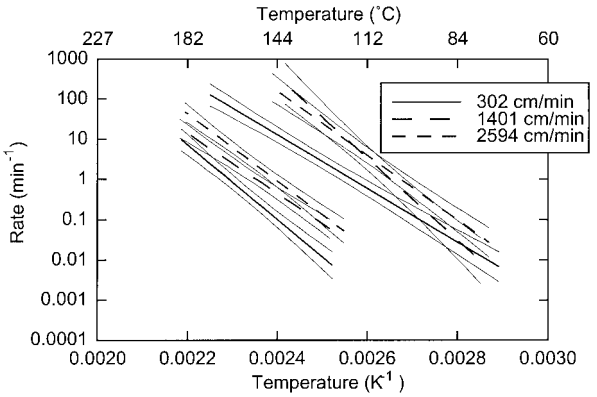

Figure 10 Arrhenius plots depicting the effect of draw velocity. The rise curves lie above the decay curves. The fibers were all fabricated at a melt temperature of 219°C and extrusion velocity of 0.0127 cm/min. The draw velocities are as shown in the legend.

Entropic springs

Rubber elastomers have also been called entropic springs because of the fact that the force developed in them is attributed to the entropy in the system. According to classical rubber elasticity theory, the force developed in an elastomer consists of two components, an enthalpic and entropic contribution,[45] and is expressed as

$$f = \left(\frac{\partial U}{\partial l}\right)_T + T\left(\frac{\partial f}{\partial T}\right)_l \tag{8}$$

where

$$-\left(\frac{\partial S}{\partial l}\right)_T = \left(\frac{\partial f}{\partial T}\right)_l \tag{9}$$

Theoretically, the slope of the force versus temperature relationship will yield the change in entropy of the system. Generally, the force increases with temperature for an elastomer. The results presented earlier, however, show that maximum stress was basically constant with respect to temperature. For some fiber systems, the maximum stress decreased at high temperatures (see Fig. 6), but this was not seen consistently. At low temperatures (<100°C), the maximum stress neither consistently increased nor decreased (e.g., Fig. 6), and previous work with other PMMA fibers showed that the maximum stress remained constant to the lowest temperature tested (65°C).[43] The temperatures that were tested were the highest possible using the data-acquisition system. To test higher temperatures, a faster data-acquisition system would need to be used, and the application of heat would need to take less than the 2–3 s it currently takes. To test lower temperatures, it would be recommended to reduce the number of fiber types and samples, given that each test at temperatures < 100°C takes 3 to 7 days. It is possible that our results do not agree with classical rubber elasticity theory because our fibers are much more highly oriented than typical rubber elastomers. At high levels of orientation, such as seen here, the entropic driving force for the fiber to relax may overshadow any temperature effects that are predicted by the classical theory. Because rubber elasticity theory has been used to explain results in other studies with PMMA at low levels of orientation,[26,29–38] a next step with this apparatus would be to fabricate fibers with lower levels of orientation than available for this study and test them in fiber shrinkage.

Although the maximum stress did not vary with temperature, there were differences seen between maximum stresses of fibers with differing amounts of retained molecular orientation. These relationships can be explored using statistical thermodynamics and classical rubber elasticity theories. For an elastomer in simple tension, the stress can be calculated as a function of the extension ratio if we assume that the chains have a Gaussian probability of having a certain configuration. When constant volume is assumed, the classical result is[45]

$$\sigma_1 = G\left(\Lambda_1 - \frac{1}{\Lambda_1^2}\right) \tag{10}$$

where σ_1 is the maximum shrinkage stress and Λ_1 is the extension ratio. The extension ratios are ratios of the stressed length to the unstressed length, or the free shrinkage of the fiber when it is heated with no constraint. This could also be expressed as the heat relaxation ratio (HRR), which is the ratio of the oriented length of fiber to the unoriented length of fiber, or

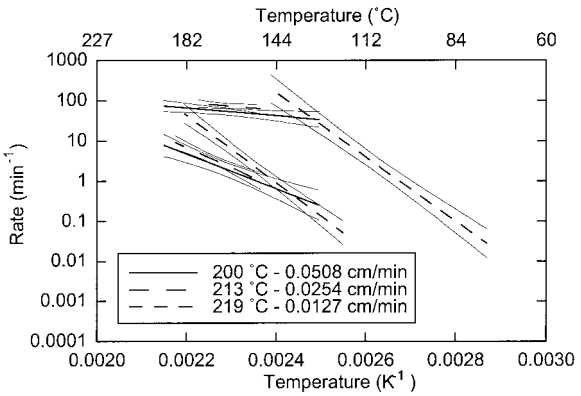

Figure 11 Arrhenius plots depicting the effect of constant viscosity. The rise curves lie above the decay curves. The fibers were all fabricated at a constant nominal viscosity of 6.3E6 Pa s. The processing conditions are as listed in the legend.

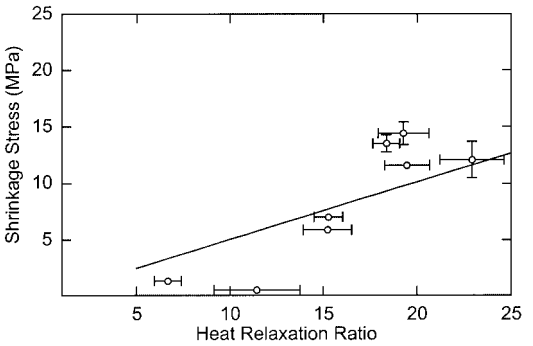

Figure 12 Fiber maximum stress versus heat relaxation ratio (HRR) for all fibers. The model presented in eq. (10) is used to plot the line through the data points, with $G = 0.507$ MPa. The correlation coefficient (R) for this line is 0.78. Data points are means ± 1SD.

length after heating.[1] This result is shown in Figure 12. The data points are shown as means ± SD, with the solid line representing the best fit through eq. (10) ($G = 0.507$ GPa). Only maximum stress values generated above oven temperatures of 100°C are included in the figure because elastomeric behavior occurs only above T_g. The correlation is quite high, considering that the fibers consist of many different fiber groups fabricated at different temperatures, draw ratios, and viscosities. To further evaluate these relationships, it would be recommended to test a wider variety of extension ratios of fibers fabricated at the same temperature to eliminate competing effects. The correlation is still quite good, however, indicating that the maximum stresses developed in the fibers during heating can be correlated to rubber elasticity effects. One possible reason for deviations, particularly at high HRR values, may be because the polymer chains are beginning to slide past one another, and therefore do not contribute fully to the maximum stress developed in the fiber.

The shear modulus (G) can also be calculated by[45]

$$G = \frac{\rho RT}{M_e} \tag{11}$$

Fiber-shrinkage tests were conducted from 100 to 200°C. The free volume of the polymer increases with temperature, resulting in a decrease in density. Using data from Schmidt and Mauer,[46] the density was calculated to be 1169 kg/m^3 at 100°C and 1100 kg/m^3 at 200°C. M_e is the molecular weight between entanglements. An M_e of 8000 g/mol yields a modulus of 0.453 GPa at 100°C, and 0.540 GPa at 200°C, which bracket the modulus of 0.507 GPa calculated from the experimental data. Because the molecular weight of methyl methacrylate is 100 g/mol, crosslinks are predicted to be present every 80 mers, or 160 carbon atoms. The molecular weight of V045 was also previously characterized by gel permeation chromatography as 212,000 g/mol with a polydispersity of 8.3.[6] This would correspond to about 26 crosslinks per V045 molecule. Vulcanized rubbers have 10–20 crosslinks per molecule,[42] showing good agreement between traditional rubber elastomers and thermoplastic elastomers with crosslinks formed by entanglements of molecules. Because the polymer's polydispersity is quite high, a correction factor to the shear modulus that accounts for the loose ends could be applied[45]:

$$G = \frac{\rho RT}{M_e}\left(1 - \frac{2M_e}{M}\right) \tag{12}$$

where M_e is the molecular weight between entanglements and M is the primary molecular weight. As the molecular weight of the polymer increases, these effects are minimized. The molecular weights of the acrylic are sufficiently high to neglect these effects; however, the polydispersity of the polymers will also contribute significantly to the development of stress in the polymer fibers.

These results also show the limitations of the rubber elasticity theories. Traditionally, the stresses predicted by eq. (10) are valid only at low extension ratios. At higher extension ratios, the theory tends to predict lower stresses than observed. It is clearly seen that the stresses are low at low extension ratios, and then increase greatly, as shown in Figure 12. At higher extension ratios, the distribution of end-to-end chain lengths is no longer Gaussian. One of the conditions of the model is that the extension of the chains should be Gaussian. As more chains become oriented, however, this Gaussian relationship is no longer valid. There are mathematical constructs to deal with this, although they add complexity without additional understanding.[45] Future work should examine the low-elongation cases more thoroughly to assess the validity of the model and then expand the consideration to fibers fabricated under similar processing conditions. In this study, fibers were fabricated and tested at the widest range of HRR values available.

Relaxation and processing times

Processing of PMMA fibers and SRC–PMMA are events that occur on the molecular level. Melt spinning of a fiber requires a viscous melt of PMMA with the right properties to be extruded through a spinneret and drawn into a highly oriented fiber. During this process, the molecules are sheared, oriented, and undergo massive reorganization that is frozen in upon cooling. While SRC–PMMA is being processed, the outer portion of the fiber softens while the entire fiber is mechanically constrained, and the polymer chains in these areas bond with adjacent chains to form a network of entanglements that will bond the fibers to

one another. Fiber shrinkage Arrhenius curves yield information about the relaxation times of PMMA fibers, and existing theories and experiments may be able to help predict or explain the times found in this study.

Classical theories have been used to characterize relaxation times of monodisperse polymers in solution, such as the theory advanced by Rouse and Bueche, but are not very good at explaining events in polymer melts.[42] The reptation theory constrains the polymer chain to movements along the polymer length, but prohibits movements perpendicular to the chain length. For a monodisperse polymer melt, the assumption of a fixed tube within the gel or melt is an appropriate model. Once the polymer has relaxed from its entangled structure, the chains can reptate out of the tube, or disengage. The time for disengagement (λ_d), which can also be called a diffusion time, can be written[47]

$$\lambda_d = \frac{15 M_e \eta_0}{\pi^2 \rho R T} \tag{13}$$

For polydisperse polymers, such as those used in this study, however, the relaxation process becomes more complicated. The main factor to consider is that the shorter chains disengage first, eliminating an obstacle for further reptation of the longer chains. Because an obstacle has been removed, the tube can expand, an effect called tube dilation.[48] Tube dilation can shorten the relaxation times by making it easier for the remaining chains to move.[47] In addition, when the obstacle is removed, the long-chain tube may move into this area, an effect referred to as tube renewal.[48] The tube containing the polymer chain may also change in contour length during the time period of interest.[47]

Work by Kunz and Stamm[49] determined the relaxation times of PMMA by neutron reflection. Their work characterized a disengagement time of 1547 min and a Rouse relaxation time of 48 min for a molecular weight of 85,500 g/mol at 130°C. Liu et al.[50] characterized the movement of PMMA molecules by using gold markers. This work showed that for a molecular weight of 194,000 g/mol (polydispersity = 1.03), Rouse relaxation times of 4.0 min and disengagement time of 288.3 min at 145°C were obtained.

In the current work, relaxation times are much shorter. For V045 fibers fabricated at 219°C and a draw velocity of 2594 cm/min, time constants for the rise and decay are found to be 0.0054 and 0.93 min, respectively, at 145°C. At 130°C, these times are 0.029 for the rise and 5.2 min for the decay. These times are much smaller than those predicted by Kunz and Liu in their work. There are two reasons for this. First, the polydispersity of these polymers is much higher than that in the studies by Kunz and Liu. This results in shorter relaxation times as the shorter chains disengage from the network. As the shorter chains diffuse out of the polymer network, they cease to contribute to the maximum stress developed, and thus the rise and decay of the maximum stress would happen more quickly for a polydisperse polymer.

The other effect contributing to the development of maximum stress in the heated fiber is attributed to the orientation in the fiber. In an oriented fiber, the polymer chains want to return to their amorphous state as soon as thermal energy is imparted to them. Therefore, measurements of fiber shrinkage measure not only the diffusion of the molecules, but also their energetic desire to return to a high entropy state. This differentiates these experiments from traditional studies because traditional studies measure the movement of markers within an amorphous polymer.

These results can hypothetically be applied to composite processing by hot compaction. It is desired to process composites with the maximum amount of retained molecular orientation, given that polymer orientation leads to increased strength in the composite. The disengagement times of polymer molecules are related to the decay time constants. These, therefore, represent the theoretical maximum times to process composites. The difference between the rise and decay curves would theoretically represent the processing window. The rise times represent the initiation of chain motion, which would be necessary to begin composite processing; however, to retain molecular orientation, processing times would need to be chosen that are less than the decay times. Hypothetically, these concepts can help design rational hot-compaction processing methods for polymeric fibers.

CONCLUSIONS

A device was built to measure the stress generated in a heated fiber, and the time development and decay of this stress. The apparatus detected differences among fibers fabricated at a variety of processing conditions. Maximum stresses for melt-spun fibers increased with increasing retained molecular orientation, draw velocity, or decreasing fiber draw temperature. These maximum stresses correlate with the classical rubber elasticity theories when plotted versus the extension ratio of the fiber (HRR).

The rate of decay of the maximum shrinkage stress was a more subtle difference. The effects were most clearly seen in the effects of draw temperature and draw velocity. At the lowest draw temperature (187°C), the rate of stress decay was higher than that for the higher temperatures (219 or 238°C). As the draw velocity increased for V045 fibers fabricated at 219°C, the rate of stress decay also increased. Activation energies were also measured for the decay and

rise processes, and these agree well with values predicted by rheological experiments.

The authors gratefully acknowledge the donation of the Atohaas acrylic and the assistance of Zimmer, Inc. in the fiber-spinning portion of the work. The funding of the American Association for University Women in the form of a Selected Professions Fellowship was also greatly appreciated (D.D.W.). David Grecek assisted in building the fiber-shrinkage apparatus.

References

1. Buckley, C. A.; Lautenschlager, E. P.; Gilbert, J. L. J Appl Polym Sci 1992, 44, 1321.
2. Wright, D. D.; Lautenschlager, E. P. Gilbert, J. L. J Biomed Mater Res 2002, 63, 152.
3. Gilbert, J. L.; Ney, D. S.; Lautenschlager, E. P. Biomaterials 1995, 16, 1043.
4. Wright, D. D.; Lautenschlager, E. P.; Gilbert, J. L. J Biomed Mater Res 1998, 43, 153.
5. Wright, D. D.; Lautenschlager, E. P.; Gilbert, J. L. J Mater Sci Mater Med 1999, 10, 503.
6. Wright, D. D.; Lautenschlager, E. P.; Gilbert, J. L. J Biomed Mater Res 1997, 36, 441.
7. Bonner, M. J.; Hine, P. J.; Ward, I. M. Plast Rubber Compos Process Technol 1998, 27, 58.
8. Kabeel, M. A.; Bassett, D. C.; Olley, R. H.; Hine, P. J.; Ward, I. M. J Mater Sci 1994, 29, 4694.
9. Kabeel, M. A.; Bassett, D. C.; Olley, R. H.; Hine, P. J.; Ward, I. M. J Mater Sci 1995, 30, 601.
10. Morye, S. S.; Hine, P. J.; Duckett, R. A.; Carr, D. J.; Ward, I. M. Compos Part A: Appl Sci Manuf 1999, 30, 649.
11. Olley, R. H.; Bassett, D. C.; Hine, P. J.; Ward, I. M. J Mater Sci 1993, 28, 1107.
12. Tissington, B.; Pollard, G.; Ward, I. M. J Mater Sci 1991, 26, 82.
13. Ward, I. M. Plast Rubber Compos Process Appl 1993, 19, 7.
14. Woods, D. W.; Ward, I. M. Polymer 1994, 29, 2572.
15. Rasburn, J.; Hine, P. J.; Ward, I. M.; Olley, R. H.; Bassett, D. C.; Kabeel, M. A. J Mater Sci 1995, 30, 615.
16. Abo El-Maaty, M. I.; Bassett, D. C.; Olley, R. H.; Hine, P. J.; Ward, I. M. J Mater Sci 1996, 31, 1157.
17. Hine, P. J.; Ward, I. M.; Olley, R. H.; Bassett, D. C. J Mater Sci 1993, 28, 316.
18. Bechev, C. Polym Test 1995, 14, 163.
19. Göschel, U. Polymer 1996, 37, 4049.
20. Gupta, V. B.; Radhakrishnan, J.; Sett, S. K. Polymer 1994, 35, 2560.
21. Hotter, J. F.; Cuculo, J. A.; Tucker, P. A.; Annis, B. K. J Appl Polym Sci 1998, 69, 2115.
22. Lim, J. Y.; Kim, S. Y. J Polym Sci Part B: Polym Phys 2001, 39, 964.
23. Selivansky, D. Thermochim Acta 1988, 134, 283.
24. Song, R.; Lin, X.; Gao, J.; Fan, Q. Polym Bull 1998, 40, 773.
25. Bassingny, V.; Séguéla, R.; Rietsch, F.; Jasse, B. Polymer 1993, 34, 4052.
26. Ward, I. M. Polym Eng Sci 1984, 24, 724.
27. Qian, B.; Hu, P.; He, J.; Zhao, J. X.; Wu, C. Polym Eng Sci 1992, 32, 1290.
28. Buchanan, D. R. Thermomechanical Responses of Fibres: Advances in Fibre Science; Textile Institute: Manchester, UK, 1992; pp. 87–113.
29. Arruda, E. M.; Boyce, M. C.; Quintas-Bosz, H. Int J Plast 1993, 9, 783.
30. Botto, P. A.; Duckett, R. A.; Ward, I. M. Polymer 1987, 28, 257.
31. Hasan, O. A.; Boyce, M. C. Polymer 1993, 34, 5085.
32. Hope, P. S.; Ward, I. M. J Mater Sci 1981, 16, 1511.
33. Kahar, N.; Duckett, R. A.; Ward, I. M. Polymer 1978, 19, 136.
34. Kashiwagi, M.; Folkes, M. J.; Ward, I. M. Polymer 1971, 12, 697.
35. Milagin, M. F.; Shishkin, N. I. Polym Sci USSR 1988, 30, 2398.
36. Wang, L.-H.; Choy, C. L.; Porter, R. S. J Polym Sci Part B: Polym Phys 1983, 21, 657.
37. Zhao, Y.; Jasse, B.; Monnerie, L. Polym Commun 1990, 31, 395.
38. Biswas, P. K.; Sengupta, S.; Basu, A. N. Colloid Polym Sci 1988, 266, 501.
39. King, A. L. J Appl Phys 1947, 18, 595.
40. Wright, D. D.; Lautenschlager, E. P.; Gilbert, J. L. In: Transactions of the 23rd Annual Meeting of the Society for Biomaterials, New Orleans, LA, 1997; p. 263.
41. Wright, D. D.; Lautenschlager, E. P.; Gilbert, J. L. In: Transactions of the Fifth World Biomaterials Congress, Toronto, Canada, 1996.
42. Sperling, L. H. Introduction to Physical Polymer Science, John Wiley and Sons, Inc., New York 1992.
43. Wright, D. D.; Lautenschlager, E. P.; Gilbert, J. L. In: Transactions of the 25th Annual Meeting of the Society for Biomaterials, Providence, RI, 1999; p. 467.
44. Wright, D. D. Optimization and Thermomechanical Characterization of Highly Oriented PMMA Fibers and Self-Reinforced Composite PMMA; Northwestern University: Chicago, IL, 1999.
45. Treloar, L. R. G. The Physics of Rubber Elasticity; Oxford University Press: London, 1975.
46. Schmidt, M.; Maurer, F. H. J. J Polym Sci Part B: Polym Phys 1998, 36, 1061.
47. Dealy, J. M.; Wissbrun, J. F. Melt Rheology and Its Role in Plastics Processing: Theory and Applications; Van Nostrand Reinhold: New York, 1990.
48. Doi, M.; Graessley, W. W.; Helfand, E.; Pearson, D. S. Macromolecules 1987, 20, 1900.
49. Kunz, K.; Stamm, M. Macromolecules 1996, 29, 2548.
50. Liu, Y.; Reiter, G.; Kunz, K.; Stamm, M. Macromolecules 1993, 26, 2134.